A thermodynamic framework for modelling membrane transporters using bond graphs

Michael Pan[1], Peter J. Gawthrop[1], Kenneth Tran[2], Joseph Cursons[3,4], Edmund J. Crampin[1,5,6,*]

[1]Systems Biology Laboratory, School of Mathematics and Statistics, and Department of Biomedical Engineering, Melbourne School of Engineering, University of Melbourne, Parkville, Victoria 3010, Australia

[2]Auckland Bioengineering Institute, University of Auckland

[3]Bioinformatics Division, Walter and Eliza Hall Institute of Medical Research, Parkville, Victoria 3052, Australia

[4]Department of Medical Biology, School of Medicine, University of Melbourne, Parkville, Victoria 3010, Australia

[5]School of Medicine, Faculty of Medicine, Dentistry and Health Sciences, University of Melbourne, Parkville, Victoria 3010

[6]ARC Centre of Excellence in Convergent Bio-Nano Science and Technology, Melbourne School of Engineering, University of Melbourne, Parkville, Victoria 3010, Australia

*Corresponding author. Email: edmund.crampin@unimelb.edu.au

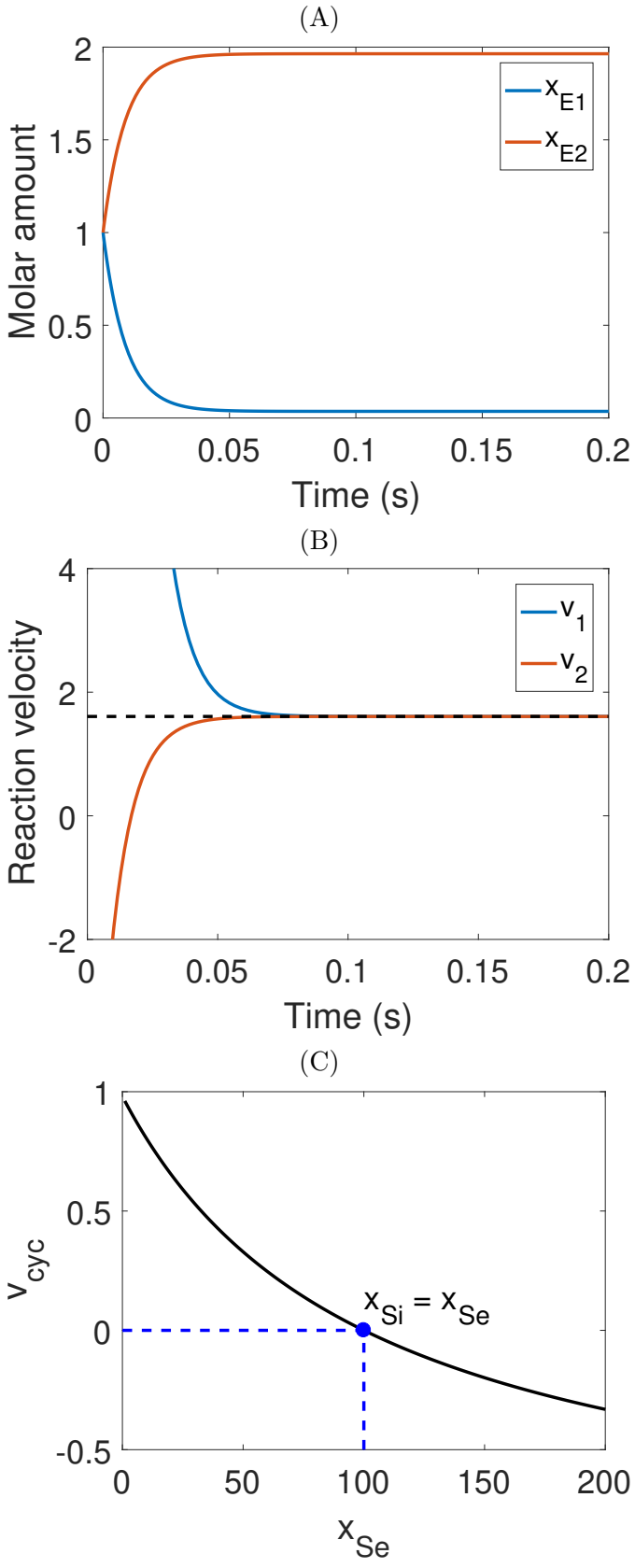

Figure 1: Enzyme cycle model. A passive transporter can be modelled using the enzyme cycle $E_1 + S_i \rightleftharpoons E_2 \rightleftharpoons E_2 + S_e$. We simulate this model, and plot how the enzyme states **(A)** and reaction velocities **(B)** change with respect to time. **(C)** The transporter reaches a steady state, with the direction of steady-state transport dictated by the concentration gradient of the substrate.

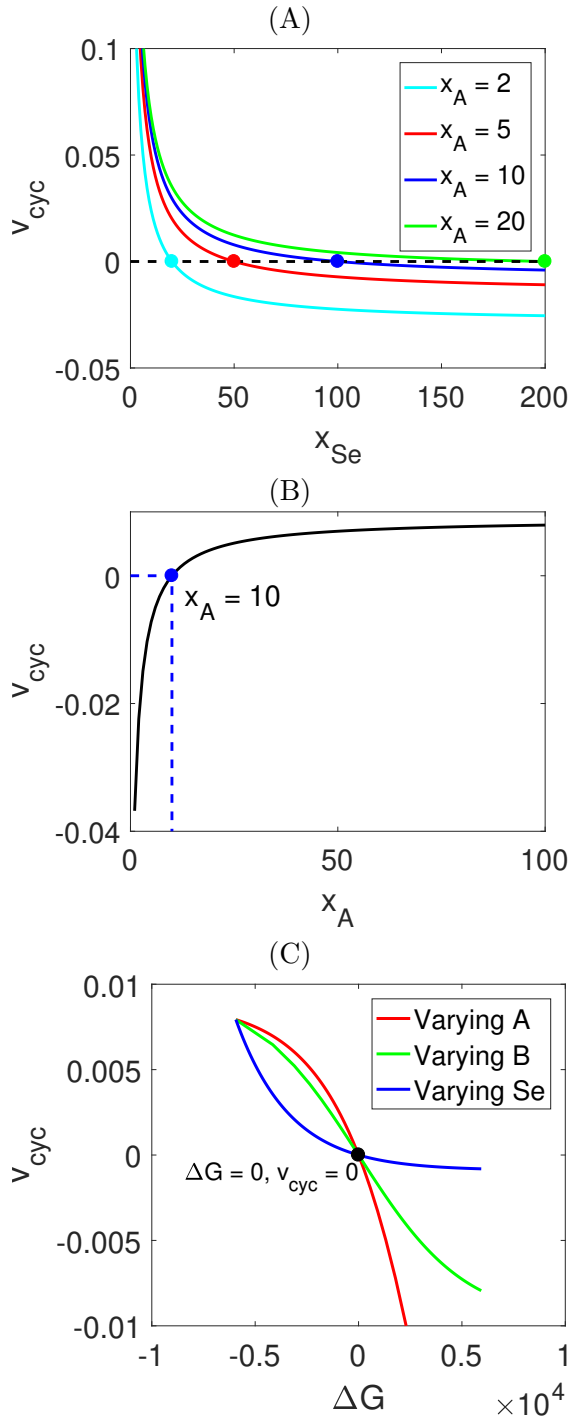

Figure 2: Coupled transport. In order for a transporter to move a substrate against a concentration gradient, it must couple the transport to a process that generates sufficient energy for the transport to occur. Here we model a transporter that couples the transport of substrate to another biochemical reaction $\mathrm{A} \rightleftharpoons \mathrm{B}$, giving rise to the overall reaction $\mathrm{S_i} + A \rightleftharpoons \mathrm{S_e} + B$. We simulate this system to steady state. The plots show that the amount of A affects the ability of the transporter to move a substrate against a chemical gradient, shifting the equilibrium point to a higher concentration of Se **(A)** and increasing the cycling rate **(B)**. **(C)** By modelling this system as a bond graph, fundamental thermodynamic constraints are captured, therefore the pump only operates in the direction of decreasing chemical potential, and stops cycling at equilibrium.

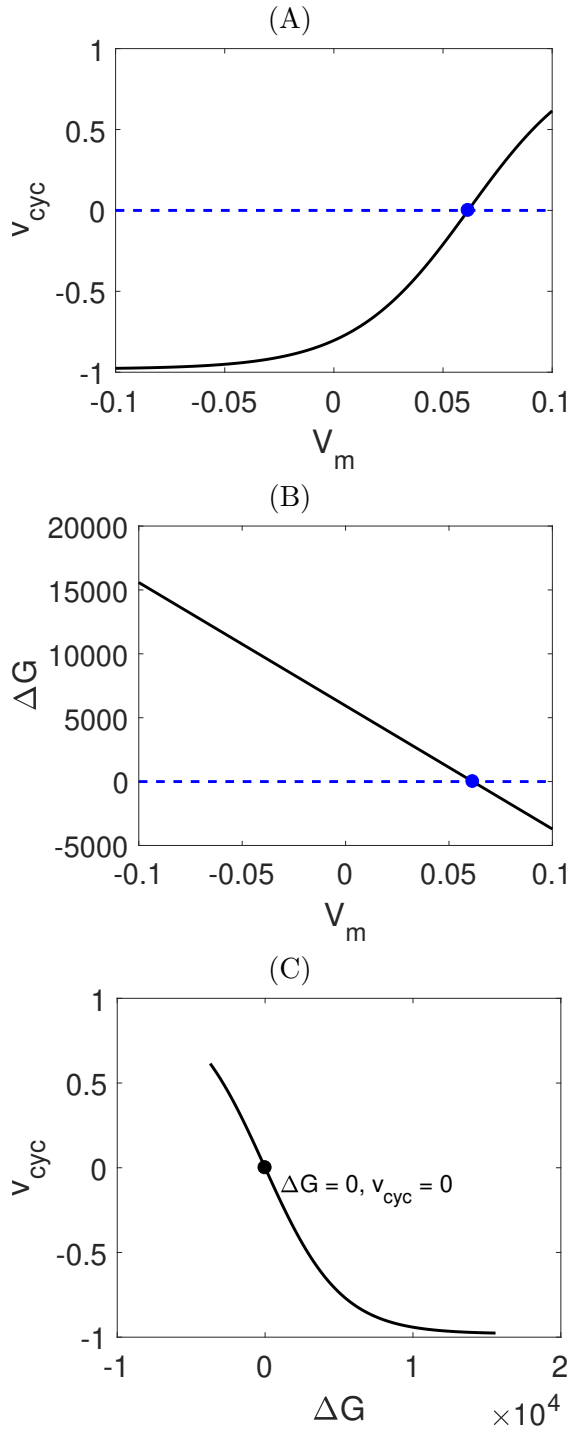

Figure 3: Electrogenic transport. Many transporters, including ion transporters, move charged species across a membrane that is charged. For these transporters, the membrane potential contributes to the thermodynamics and kinetics of the system. Because bond graphs are domain-independent, they are able to model the interaction between chemical and electrochemical power in electrogenic systems. Here we simulate the transporter model $E_1 + S_i^+ \rightleftharpoons E_2 \rightleftharpoons E_2 + S_e^+$, where the substrate is charged. **(A)** A plot of the cycling rate against voltage shows the bond graph model captures the equilibrium point (Nernst potential) of this transporter. **(B)** The membrane voltage has a linear contribution to the Gibbs free energy of the transporter. **(C)** Plotting cycling rate against Gibbs free energy verifies that the equilibrium point corresponds to a Gibbs free energy of zero.

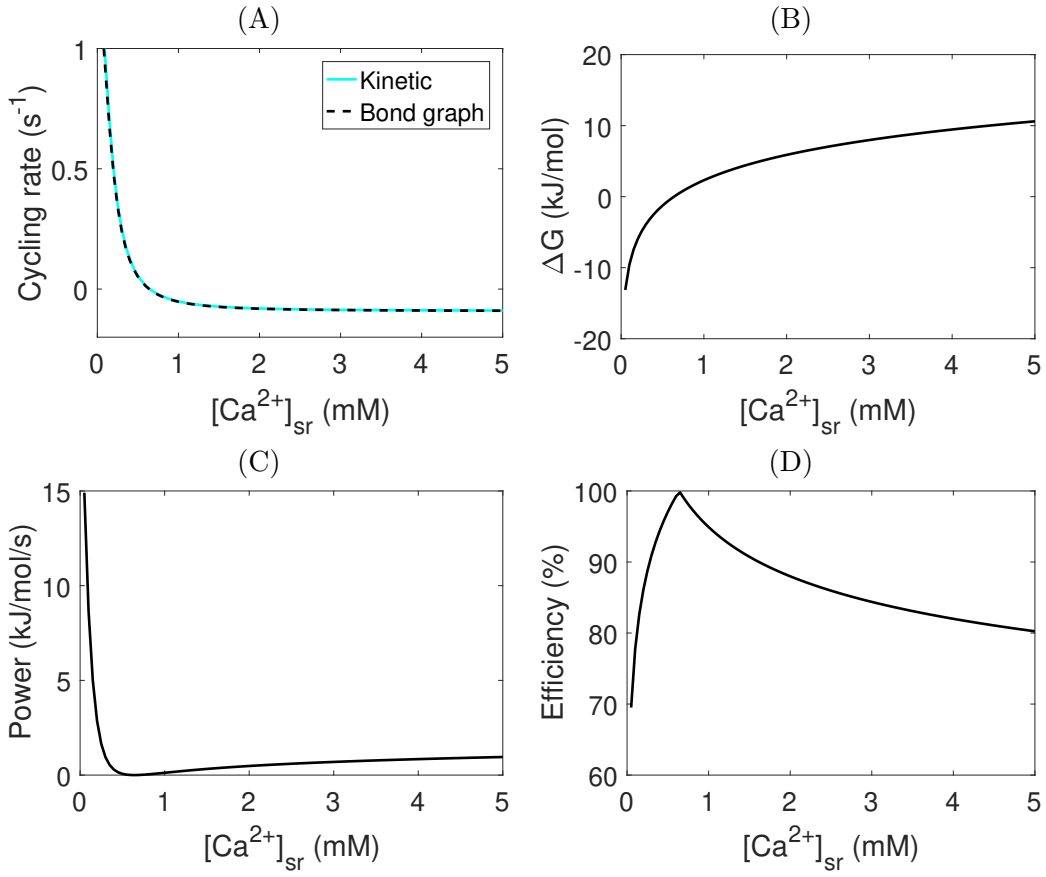

Figure 4: Simulation of the SERCA pump. **(A)** Comparison of cycling rates for kinetic and bond graph models, reproducing part of Fig. 13 in Tran et al. (2009); **(B)** Gibbs free energy; **(C)** Power consumption per mol of pump; **(D)** Pump efficiency. Simulations were run with $[Ca^{2+}]_i = 150$ nM, pH = 4, [MgADP] = 0.0363 mM, [MgATP] = 0.1 mM, [Pi] = 15 mM. Cycling rates were estimated by initialising each pump state to 1/9 fmol, and running the simulation to its steady state.

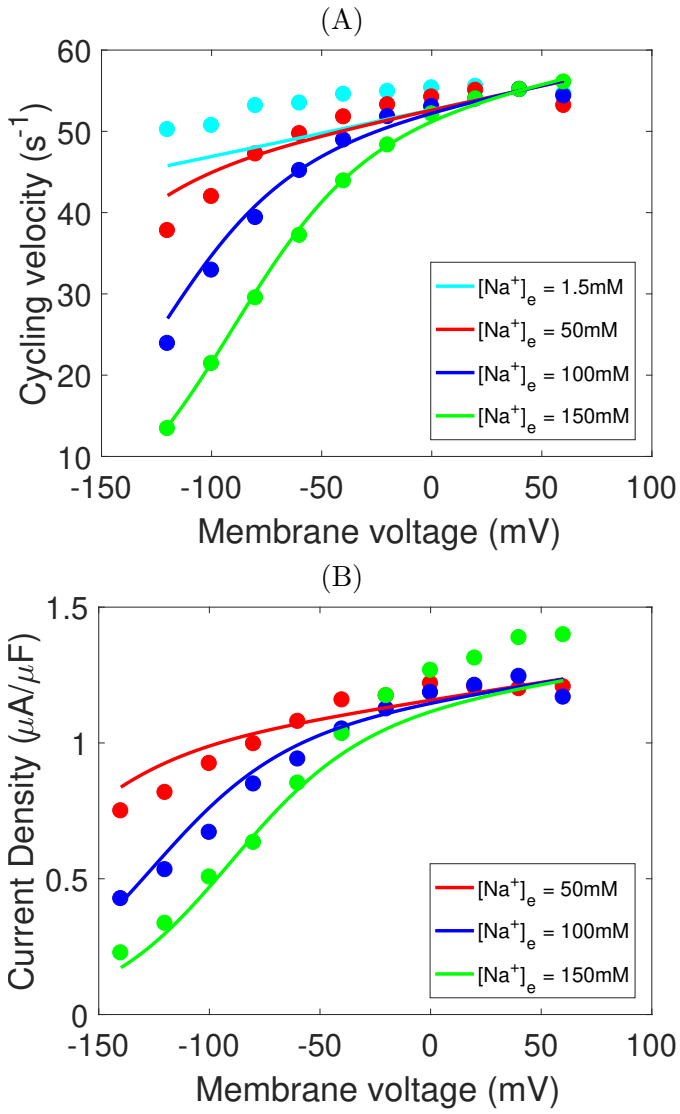

Figure 5: Fit of the cardiac Na^+/K^+ ATPase model to current-voltage measurements. (A) Comparison of the model to extracellular sodium and voltage data (Nakao and Gadsby, 1989, Fig. 3), with cycling velocities scaled to a value of 55 s^{-1} at $V = 40$ mV. **(B)** Comparison of the model to whole-cell current measurements (Nakao and Gadsby, 1989, Fig. 2A). $[Na^+]_i = 50$ mM, $[K^+]_i = 0$ mM, $[K^+]_e = 5.4$ mM, pH = 7.4, $[Pi]_{tot} = 0$ mM, [MgATP] = 10 mM, [MgADP] = 0 mM, $T = 310$ K.

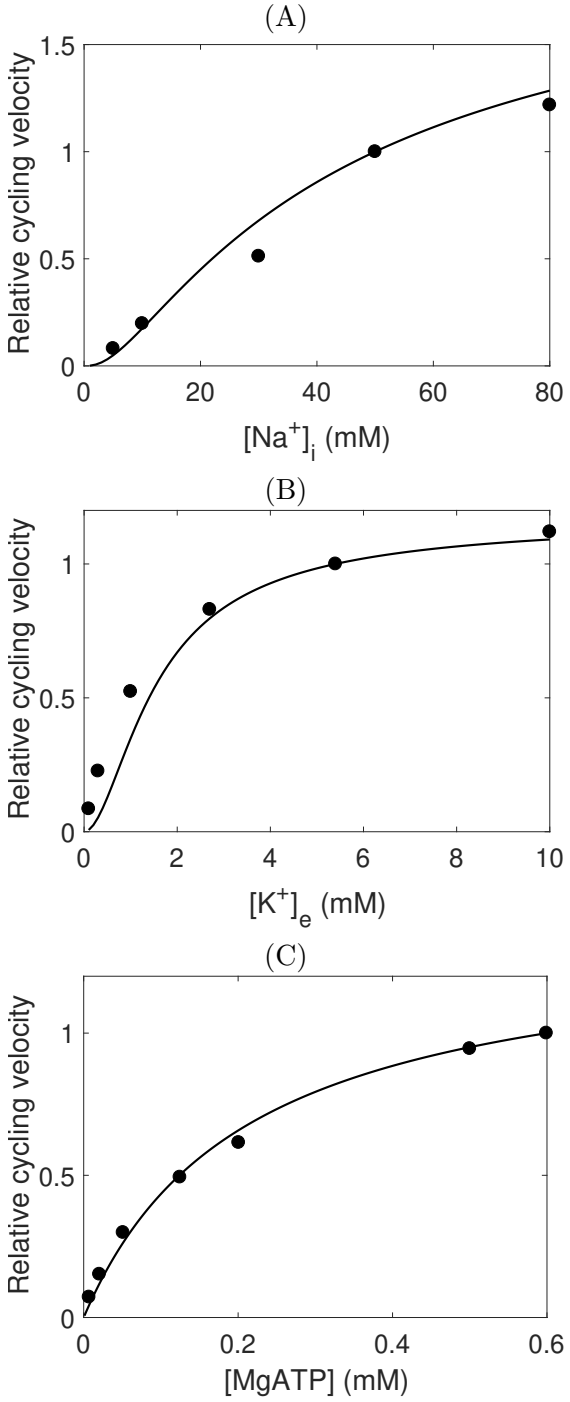

Figure 6: Fit of the cardiac Na^+/K^+ ATPase model to metabolite dependence data. (A) Comparison of the model to data with varying intracellular sodium concentrations (Hansen et al., 2002, Fig. 7A), normalised to the cycling velocity at $[Na^+]_i = 50$ mM. **(B)** Comparison of the model to data with varying extracellular potassium (Nakao and Gadsby, 1989, Fig. 11A), normalised to the cycling velocity at $[K^+]_e = 5.4$ mM. **(C)** Comparison of the model to data with varying ATP (Friedrich et al., 1996, Fig. 3B), normalised to the cycling velocity at [MgATP] = 0.6 mM.

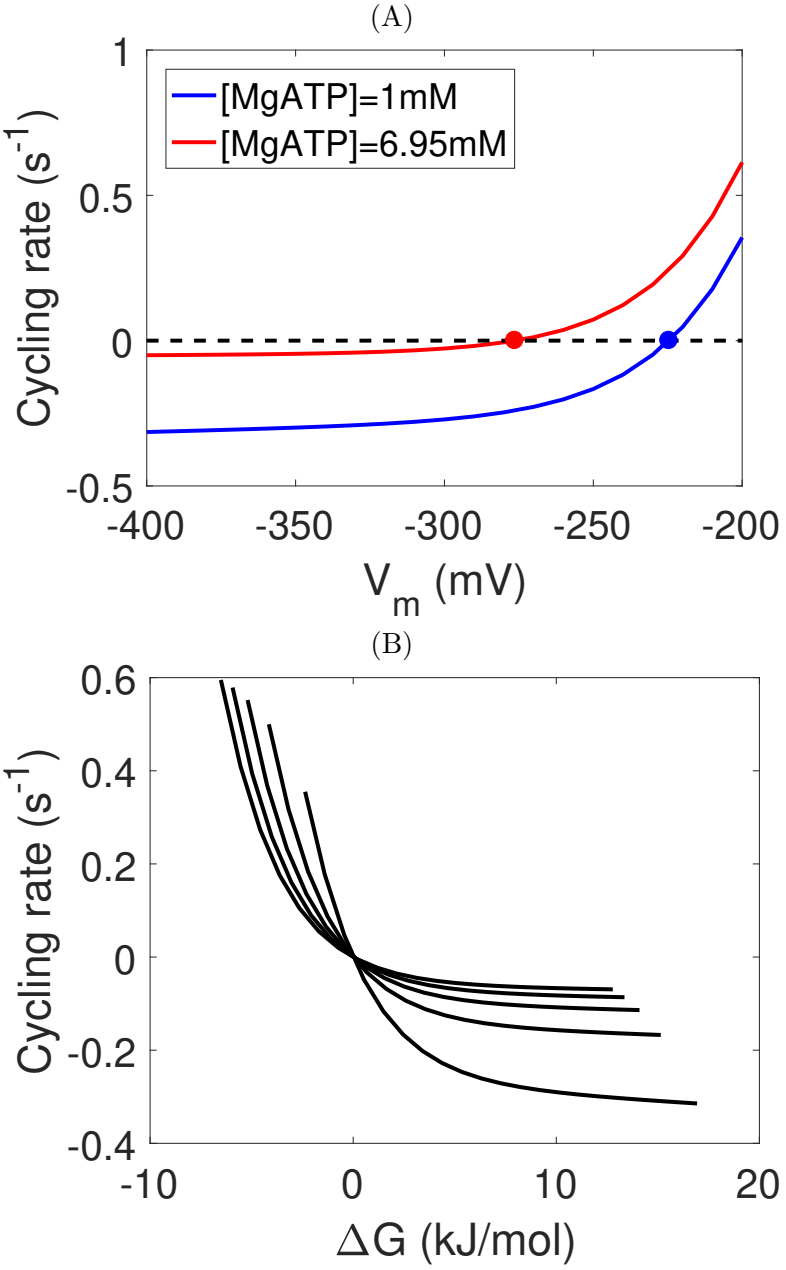

Figure 7: Simulation of the Na^+/K^+ ATPase. (A) Cycling rates of the pump near reversal potential; **(B)** Relationship between Gibbs free energy and cycling rate. The curves represent different concentrations of MgATP, from a concentration of 1 mM on the right, with increments of 1 mM up to a concentration of 5mM on the left. The Gibbs free energy was varied by changing the membrane potential. For (A) and (B), simulations were run using $[Na^+]_i = 10$ mM, $[Na^+]_e = 140$ mM, $[K^+]_i = 145$ mM, $[K^+]_e = 5.4$ mM, pH = 7.095, [Pi] = 0.3971 mM, [MgATP] = 6.95 mM, [MgADP] = 0.035 mM. Each pump state was initialised to 1/15 fmol, and steady states were estimated by running each simulation to steady state.